Computational Structural Engineering
An International Journal
Vol. 1, No. 1, pp. 49~57 (2001)

Computational Structural Engineering Institute

Benchmark Modal Stress-Resultant Distributions for Vibrating Rectangular Plates with Two Opposite Edges Free

Y. Xiang†, C.M. Wang[1], T. Utsunomiya[2] and C. Machimdamrong[2]

†School of Engineering and Industrial Design, University of Western Sydney, Penrith South DC, NSW 1797, Australia
[1]Department of Civil Engineering, National University of Singapore, Kent Ridge, Singapore 119260
[2]Department of Civil Engineering, Kyoto University, Kyoto 606-8501, Japan

Received December 2000; Accepted April 2001

ABSTRACT

This paper presents exact solutions for the modal stress-resultant distributions for vibrating rectangular Mindlin plates involving two opposite sides simply supported while the other two sides free. These exact stress-resultants of vibrating plates with free edges, hitherto unavailable, are very important because they serve as benchmark solutions for checking numerical solutions and methods. Using the exact solutions of a square plate, this paper highlights the problem of determining accurate stress-resultants, especially the transverse shear forces and twisting moments in thin plates, when employing the widely used numerical methods such as the Ritz method and the finite element method. Thus, this study shows that there is a need for researchers to develop refinements to the Ritz method and the finite element method for determining very accurate stress-resultants in vibrating plates with free edges.

Keywords: free edge, Levy solutions, Kirchhoff plates, Mindlin plates, modal stress distribution, vibration

1. Introduction

In the dynamic analysis of a very large floating structure (VLFS), it is crucial that the stress-resultants are accurately determined for design purposes. A box-like VLFS can be modelled as a rectangular plate vibrating freely in air (Utsunomiya *et al.*, 1998). While carrying a free vibration analysis of rectangular VLFS, the authors have found that the classical thin plate theory cannot furnish correct modal stress-resultant distributions, especially the transverse shear forces and the twisting moments along the free edges of the plate. Even the more refined Mindlin plate theory used in conjunction with the Ritz method or the finite element method encounters convergence problems for calculating the stress-resultants, especially when the plate is thin. One of the reasons for the Ritz method and the finite element method being not able to predict the stress-resultants accurately is that the natural boundary conditions are not imposed along the free edges of the plate in the numerical solution procedure. Thus, as a first step in developing a better numerical solution approach, one has to obtain closed-form solutions so that numerical solutions computed from newly developed numerical methods may be assessed for their validity, convergence and accuracy.

In the open literature, the authors could not find exact modal stress-resultant distributions for vibrating plates with free edges to compare with the numerical results. There are papers and books published on vibrating plates with free edges, but these publications only presented the vibration frequencies and mode shapes (see for example, Gorman, 1982; Gorman and Ding, 1996; Chen *et al.*, 1999). This prompted the authors to derive closed-form solutions for a rectangular Mindlin plate with two opposite edges simply supported while the other edges free (hereafter will be referred to as FSFS plate). Such a rectangular plate allows one to employ the Levy-type solution approach in determining the desired closed-form solutions. The closed-form solutions should serve as important benchmark solutions for researchers and engineers who are developing numerical methods for obtaining accurate stress-resultants in vibrating plates involving free

† Corresponding author
Tel.: +65-8742157; Fax: +65-7791635
E-mail address: y.xiang@uws.edu.au

edges.

Presented herein is the approach used to obtain the closed form results of freely vibrating FSFS Mindlin plates. Sample vibration frequencies, modal deflections and modal stress-resultants are tabulated and plotted for the first three modes of vibration of square plates with two thickness ratios. One thickness ratio represents a thin plate while the other represents a thick plate. Vibration results are also obtained from the Ritz method and the finite element method. When these latter results are compared with the closed-form solutions, one can clearly observe the inability of these widely-used numerical methods in furnishing accurate transverse shear forces and twisting moments when the plates are thin. It now remains for researchers to develop better numerical methods to capture the modal stress-resultants accurately for vibrating plates with free edges.

2. Mathematical Modelling

2.1 Governing Differential Equations

Consider a rectangular Mindlin plate of length a, width b and thickness h as shown in Fig. 1. The origin of the coordinates (x, y) is positioned as shown in Fig. 1. The governing differential equations for the plate in harmonic vibration are given by (Mindlin, 1951)

$$\kappa^2 Gh\left[\frac{\partial}{\partial x}\left(\frac{\partial w}{\partial x}+\theta_x\right)+\frac{\partial}{\partial y}\left(\frac{\partial w}{\partial y}+\theta_y\right)\right]+\rho h\omega^2 w=0 \tag{1}$$

$$D\left[\frac{\partial}{\partial x}\left(\frac{\partial \theta_x}{\partial x}+\nu\frac{\partial \theta_y}{\partial y}\right)\right]+\frac{(1-\nu)D}{2}\left[\frac{\partial}{\partial y}\left(\frac{\partial \theta_y}{\partial x}+\frac{\partial \theta_x}{\partial y}\right)\right]$$

$$-\kappa^2 Gh\left(\frac{\partial w}{\partial x}+\theta_x\right)+\frac{\rho h^3}{12}\omega^3\theta_x=0 \tag{2}$$

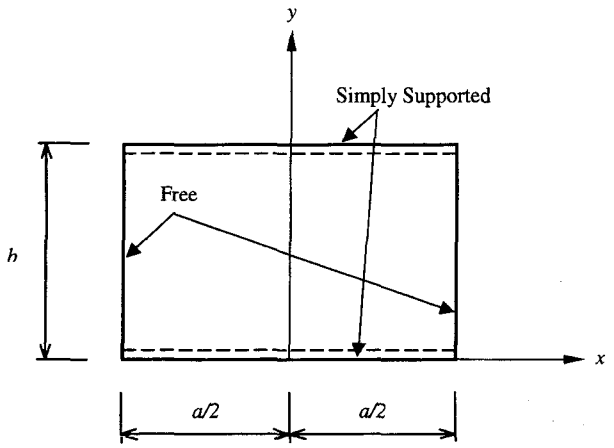

Fig. 1. Geometry and coordinate system of a rectangular plate with two edges simply supported and the other two edges free.

$$D\left[\frac{\partial}{\partial y}\left(\frac{\partial \theta_y}{\partial y}+\nu\frac{\partial \theta_x}{\partial x}\right)\right]+\frac{(1-\nu)D}{2}\left[\frac{\partial}{\partial x}\left(\frac{\partial \theta_y}{\partial x}+\frac{\partial \theta_x}{\partial y}\right)\right]$$

$$-\kappa^2 Gh\left(\frac{\partial w}{\partial y}+\theta_y\right)+\frac{\rho h^3}{12}\omega^3\theta_y=0 \tag{3}$$

where E is Young's modulus, $G = E/[2(1+\nu)]$ the shear modulus, ν the Poisson's ratio, κ^2 the shear correction factor, $G = Eh^3/[12(1+\nu^2)]$ the flexural rigidity of the plate, ρ the mass density of the plate, ω the circular frequency of the plate, w the transverse displacement, θ_x and θ_y and are rotations in the y and x directions, respectively.

In producing the closed-form solutions for the stress-resultant distributions of vibrating rectangular plates with free edges, we consider the case of the plate having two opposite edges simply supported (i.e. edges $y = 0$ and $y = b$), while the other two edges free (i.e. edges $x = \pm a/2$). The boundary conditions for the two simply supported, parallel edges ($y = 0$ and $y = b$) are

$$w = M_y = \theta_x = 0 \tag{4}$$

and the boundary conditions for the two free edges ($x = -a/2$ and $x = a/2$) are

$$M_x = M_{yx} = Q_x = 0 \tag{5}$$

in which the stress-resultants M_x, M_y, M_{yx} and Q_x are bending moments along the y and x axes, twisting moment and shear force, respectively. According to the Mindlin plate theory, these stress-resultants are related to the displacements as follows:

$$M_x = D\left(\frac{\partial \theta_x}{\partial x}+\nu\frac{\partial \theta_y}{\partial y}\right) \tag{6}$$

$$M_y = D\left(\frac{\partial \theta_y}{\partial y}+\nu\frac{\partial \theta_x}{\partial y}\right) \tag{7}$$

$$M_{xy} = \frac{D(1-\nu)}{2}\left[\frac{\partial \theta_x}{\partial y}+\frac{\partial \theta_y}{\partial x}\right] \tag{8}$$

$$Q_x = \kappa^2 Gh\left(\theta_x+\frac{\partial w}{\partial x}\right) \tag{9}$$

$$Q_y = \kappa^2 Gh\left(\theta_y+\frac{\partial w}{\partial y}\right) \tag{10}$$

2.2 Closed-form Solution Procedure

The Levy-type solution approach is employed to solve the governing differential equations for plates with the prescribed boundary conditions (Khdeir, 1988; Chen and Liu, 1990; Xiang *et al.*, 1996). The trigonometric functions are used in the displacement fields, along the y direction, to satisfy the boundary conditions at the two simply sup-

ported edges ($y = 0$ and $y = b$). The displacement fields of the plate can be expressed as

$$\begin{Bmatrix} w(x,y) \\ \theta_x(x,y) \\ \theta_y(x,y) \end{Bmatrix} = \begin{Bmatrix} \phi_w(x)\sin\frac{m\pi y}{b} \\ \phi_x(x)\sin\frac{m\pi y}{b} \\ \phi_y(x)\cos\frac{m\pi y}{b} \end{Bmatrix} \tag{11}$$

in which $\phi_w(x), \phi_x(x)$ and $\phi_y(x)$ are unknown functions along the x direction and are to be determined, and m is the number of half waves of the displacements in the y direction.

By substituting Eq. (11) into Eqs. (1) to (3), the following linear ordinary differential equation system can be derived:

$$\phi'(x) = H\phi(x) \tag{12}$$

where $\phi(x) = [\phi_w \phi_w' \phi_x \phi_x' \phi_y \phi_y']^T$ and the prime (') denotes the derivative with respect to x, and H is a 6×6 matrix with the following non-zero elements:

$$H_{12} = H_{34} = H_{56} = 1 \tag{13a}$$

$$H_{21} = \frac{(m\pi/b)^2(-\kappa^2 Gh) + \rho h\omega^2}{-k^2 Gh} \tag{13b}$$

$$H_{24} = -1,\ H_{25} = (m\pi/b) \tag{13c, d}$$

$$H_{42} = \frac{\kappa^2 Gh}{D},\ H_{46} = \frac{(m\pi/b)(1+\nu)}{2} \tag{13e, f}$$

$$H_{61} = \frac{(m\pi/b)\kappa^2 Gh}{[D(1-\nu)/2]},\ H_{64} = -\frac{(m\pi/b)(1+\nu)}{1-\nu} \tag{13h, i}$$

$$H_{65} = \frac{D(m\pi/b)^2 + \kappa^2 Gh - \rho h^3\omega^2/12}{[D(1-\nu)/2]} \tag{13j}$$

A general solution of Eq. (12) can be obtained as

$$\phi(x) = \mathbf{e}^{\mathbf{H}x}\mathbf{c} \tag{14}$$

where c is a constant column vector that can be determined by the plate boundary conditions of the two free edges and $\mathbf{e}^{\mathbf{H}x}$ is the general matrix solution of Eq. (12), given by

$$\mathbf{e}^{\mathbf{H}x} = \mathbf{Z}(x)\mathbf{Z}^{-1}(\mathbf{0}) \tag{15}$$

in which $\mathbf{Z}(x)$ is the fundamental matrix solution of Eq. (12) and $Z^{-1}(0)$ is the inverse of $\mathbf{Z}(x)$ with $x = 0$. The matrix $\mathbf{Z}(x)$ is formed from the eigenvalues and eigenvectors of matrix $\mathbf{H}$. The procedure in obtaining $\mathbf{Z}(x)$ has been detailed by Xiang *et al.* (1996).

In view of Eq. (14) and applying the boundary conditions on the two free edges ($x = \pm a/2$), a homogeneous system of equations is obtained:

$$\boldsymbol{K}\boldsymbol{c} = \mathbf{0} \tag{16}$$

The vibration frequency ω and the corresponding eigenvector $\mathbf{c}$ are determined when the determinant of $\boldsymbol{K}$ is set to zero. As the vibration frequency ω is imbedded in matrix $\mathbf{H}$, it cannot be obtained directly from Eq. (16). A numerical iteration procedure has been developed to carry out the calculations (Xiang *et al.*, 1996).

2.3 Calculation of Stress-Resultants

After the frequency ω and the corresponding eigenvector $\mathbf{c}$ are obtained from Eq. (16), the solution of $\phi(x)$, which contains the displacement fields in the x direction and their first derivatives, is determined from Eq. (14). In view of Eqs. (6) to (10), the stress-resultants M_x, M_y, M_{yx}, Q_x, and Q_y can be expressed as

$$M_x = D\left(\phi_x' - \nu\frac{m\pi}{b}\phi_y\right)\sin\frac{m\pi y}{b} \tag{17}$$

$$M_y = D\left(-\frac{m\pi}{b}\phi_y + \nu\phi_x'\right)\sin\frac{m\pi y}{b} \tag{18}$$

$$M_{yx} = \frac{D(1-\nu)}{2}\left(\frac{m\pi}{b}\phi_x + \phi_y'\right)\cos\frac{m\pi y}{b} \tag{19}$$

$$Q_x = \kappa^2 Gh(\phi_x + \phi_w')\sin\frac{m\pi y}{b} \tag{20}$$

$$Q_y = \kappa^2 Gh\left(\phi_y - \frac{m\pi}{b}\phi_w\right)\cos\frac{m\pi y}{b} \tag{21}$$

3. Results and Discussions

In this section the vibration modes and distributions of the closed-form modal stress-resultants are presented for first three modes of vibration of FSFS square plates. The thickness ratios, h/b, are taken to be 0.01 to represent the case of thin plates and 0.1 to represent the case of thick plates. The Poisson ratio $\nu = 0.3$ and the shear correction factor $\kappa^2 = 5/6$ are adopted in the computations. The modal stress-resultants based on Kirchhoff (thin) and Mindlin (thick) plate theories are determined from using both the Ritz method and the finite element method (FEM). The results are presented for some selected cases.

The maximum transverse displacement of the plate in vibration is first normalised by setting

$$|w_{max}/b| = 1 \tag{22}$$

The corresponding modal stress-resultants in the plate are presented in their non-dimensional forms as follows:

$$\overline{M}_x = \frac{b}{D}M_x \tag{23}$$

$$\overline{M}_y = \frac{b}{D}M_y \tag{24}$$

Table 1. Vibration frequency parameters $\lambda = (\omega b^2/\pi^2)\sqrt{\rho h/D}$ for FSFS square plate obtained from different solution methods.

Method	h/b	Mode		
		1	2	3
Closed-Form Solution	0.01	0.9754	1.6309	3.7092
Ritz Thin Plate Solution	–	0.9759	1.6348	3.7211
Ritz Thick Plate Solution	0.01	0.9755	1.6324	3.7139
FEM Thin Plate Solution	–	0.9759	1.6346	3.7204
FEM Mindlin Plate Solution	0.01	0.9754	1.6310	3.7099
Closed-Form Solution	0.1	0.9565	1.5592	3.4307
Ritz Mindlin Plate Solution	0.1	0.9565	1.5593	3.4307
FEM Mindlin Plate Solution	0.1	0.9603	1.5725	3.5032

$$\overline{M}_{xy} = \frac{b}{D} M_{yx} \tag{25}$$

$$\overline{Q}_x = \frac{b^2}{D} Q_x \tag{26}$$

$$\overline{Q}_y = \frac{b^2}{D} Q_y \tag{27}$$

3.1 Vibration Frequencies

Table 1 presents the vibration frequency parameters $\lambda = (\omega b^2/\pi^2)\sqrt{\rho h/D}$ for the FSFS square plate using different solution methods. Note that the closed-form solutions are obtained on the basis of the Mindlin plate theory and the proposed analytical method described above. The automated p-Ritz method (Liew *et al.*, 1998) based on both the Kirchhoff (thin) and the Mindlin (thick) plate theories are used to generate the Ritz solutions. The degree of polynomial terms used to approximate the displacements in the Ritz methods is 14. The NASTRAN finite element package is also used to solve the vibration problem. These FEM solutions are obtained using two shell elements, one that is based on the Kirchhoff (thin) plate theory while the other on the Mindlin (thick) plate theory. The mesh discretization is taken as 100x100 uniform mesh with 8 noded quadrilateral element (QUAD8).

Table 1 shows that the frequency parameters obtained using the Ritz method (based on the Mindlin plate theory) are almost identical to results from the closed-form solution for a thick plate ($h/b = 0.1$). The FEM Mindlin plate results for a thick plate ($h/b = 0.1$) are not as accurate when compared to the Ritz Mindlin plate results. For the plate with $h/b = 0.01$, the Ritz and FEM results based on the Mindlin plate theory are closer to the closed-form solutions than the ones based on the Kirchhoff plate theory. This is because the thickness ratio $h/b = 0.01$ is not thin enough for the Mindlin plate solutions to approach the Kirchhoff plate solutions.

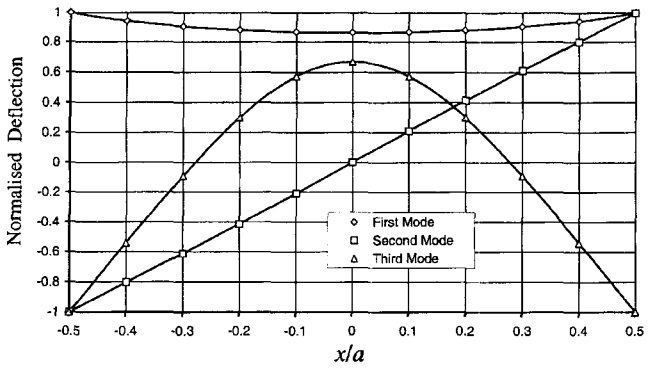

Fig. 2. Closed-form solution of normalised deflections versus the coordinate x/a for thin *FSFS* square plate ($h/b = 0.01$) vibrating in the first three modes. The deflections are taken at $y/b = 0.5$.

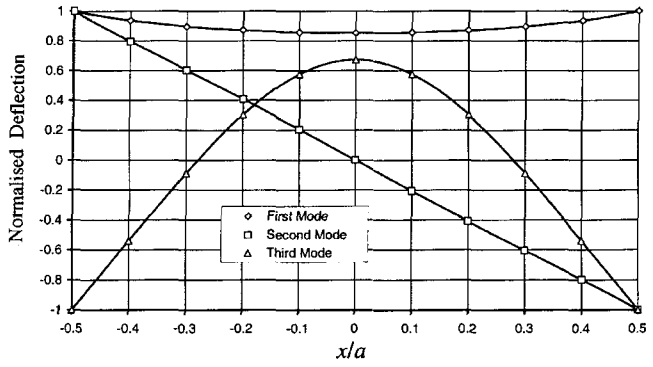

Fig. 3. Closed-form solution of normalised deflections versus the coordinate x/a for thick *FSFS* square plate ($h/b = 0.1$) vibrating in the first three modes. The deflections are taken at $y/b = 0.5$.

3.2 Mode Shapes

Figs. 2 and 3 present the vibration mode shapes for the thin and thick, square FSFS plates along the x axis with $y = b/2$. The plates are vibrating in their first three modes. The corresponding mode shapes for the thin and thick plates are very close to each other. It is found that for all three modes, the value of m (see Eq. (11)) is equal to unity. It means that there is only one half-wave for the mode shapes along the y direction. These figures also show that the mode shapes for the first and third modes are symmetric while the mode shape for the second mode is anti-symmetric. There are no nodal lines for the first mode, one nodal line for the second mode and two nodal lines for the third mode in the y direction, respectively.

3.3. Closed-Form Solutions of Modal Stress-Resultants

Figs. 4 to 8 present the closed-form solutions of modal stress-resultants, namely, shear forces $\overline{Q}_x$ and $\overline{Q}_y$, bending moments $\overline{M}_x$ and $\overline{M}_y$ and twisting moment $\overline{M}_{xy}$, for thin

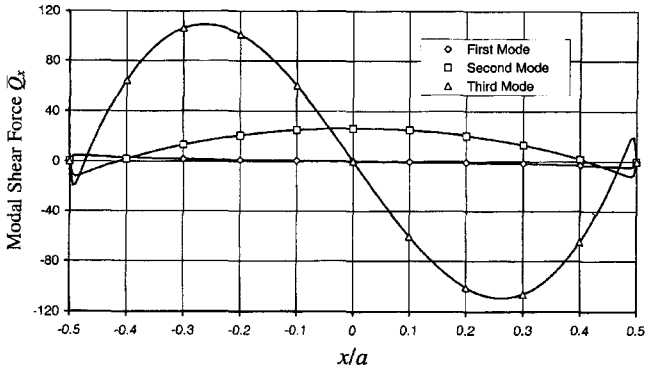

Fig. 4. Closed-form solution of modal shear force $\bar{Q}_x$ versus the coordinate x/a for thin *FSFS* square plate ($h/b = 0.01$) vibrating in the first three modes. The shear force $\bar{Q}_x$ is taken at $y/b = 0.5$.

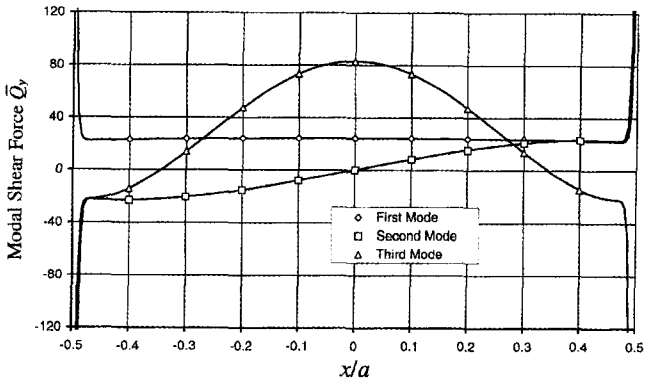

Fig. 5. Closed-form solution of modal shear force $\bar{Q}_y$ versus the coordinate x/a for thin *FSFS* square plate ($h/b = 0.01$) vibrating in the first three modes. The shear force $\bar{Q}_y$ is taken at $y/b = 0$.

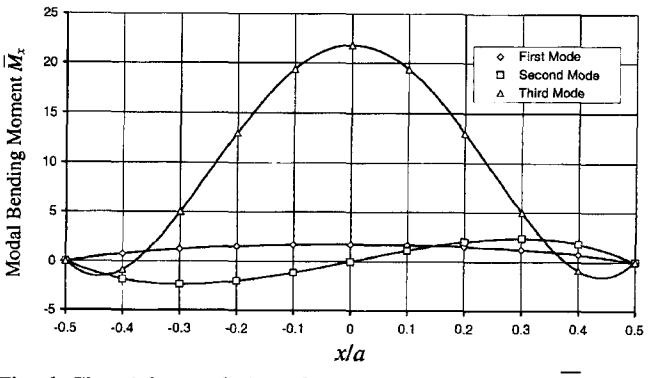

Fig. 6. Closed-form solution of modal bending moment $\bar{M}_x$ versus the coordinate x/a for thin *FSFS* square plate ($h/b = 0.01$) vibrating in the first three modes. The bending moment $\bar{M}_x$ is taken at $y/b = 0.5$.

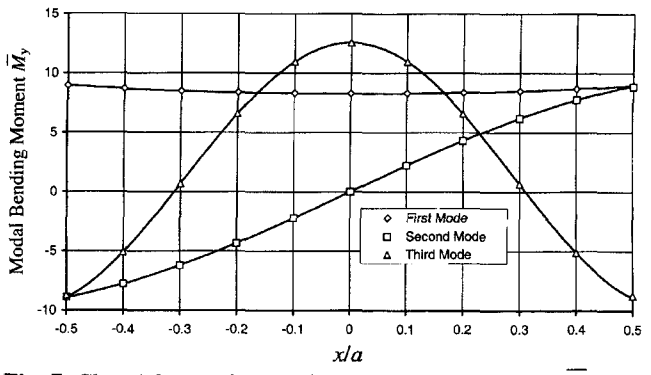

Fig. 7. Closed-form solution of modal bending moment $\bar{M}_y$ versus the coordinate x/a for thin *FSFS* square plate ($h/b = 0.01$) vibrating in the first three modes. The bending moment $\bar{M}_y$ is taken at $y/b = 0.5$.

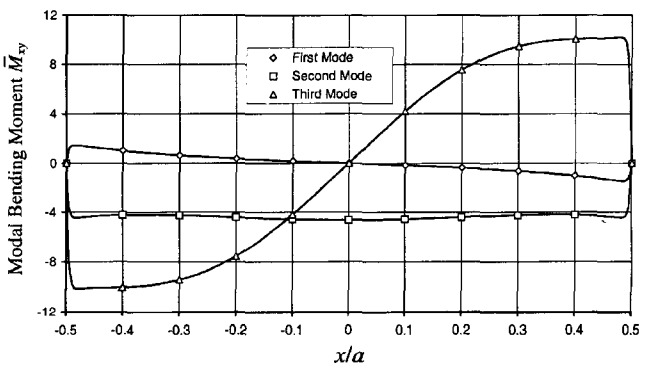

Fig. 8. Closed-form solution of modal twisting moment $\bar{M}_y$ versus the coordinate x/a for thin *FSFS* square plate ($h/b = 0.01$) vibrating in the first three modes. The twisting moment $\bar{M}_{xy}$ is taken at $y/b = 0$.

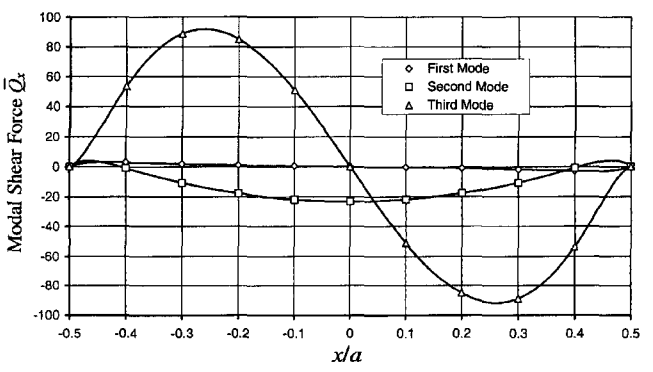

Fig. 9. Closed-form solution of modal shear force $\bar{Q}_x$ versus the coordinate x/a for thick *FSFS* square plate ($h/b = 0.1$) vibrating in the first three modes. The shear force $\bar{Q}_x$ is taken at $y/b = 0.5$.

($h/b = 0.01$) FSFS square plates vibrating in their first three modes. Figs. 9 to 13 show the stress-resultants for thick ($h/b = 0.1$) FSFS square plates.

The closed-form solutions show that the stress-resultants $\bar{Q}_x$, $\bar{M}_x$, and $\bar{M}_{xy}$ for all modes are equal to zero along the two free edges ($x = -a/2$ and $x = a/2$) (see Figs. 4, 6, 8, 9, 11 and 13). It is required by the natural boundary conditions of the plate along the free edges as defined by Eq. (5). For stress-resultants $\bar{Q}_x$, $\bar{Q}_y$ and $\bar{M}_{xy}$, there are sharp increases in the vicinity of the free edges, especially when

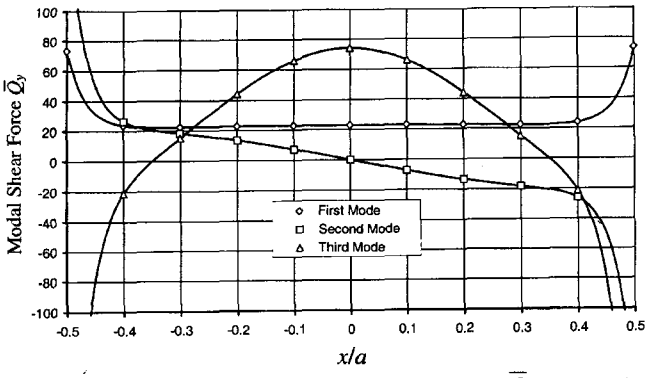

Fig. 10. Closed-form solution of modal shear force $\bar{Q}_y$ versus the coordinate x/a for thick *FSFS* square plate ($h/b = 0.1$) vibrating in the first three modes. The shear force $\bar{Q}_y$ is taken at $y/b = 0$.

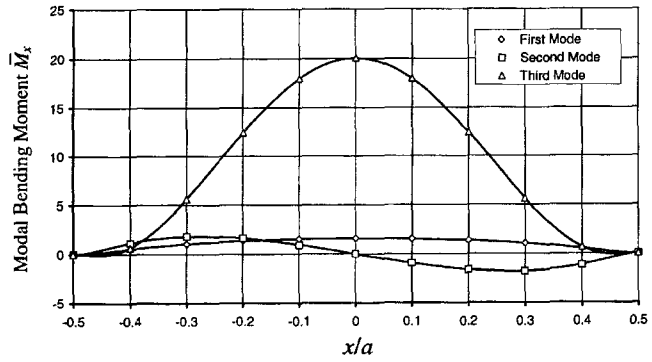

Fig. 11. Closed-form solution of modal bending moment $\bar{M}_x$ versus the coordinate x/a for thick *FSFS* square plate ($h/b = 0.1$) vibrating in the first three modes. The bending moment $\bar{M}_x$ is taken at $y/b = 0.5$.

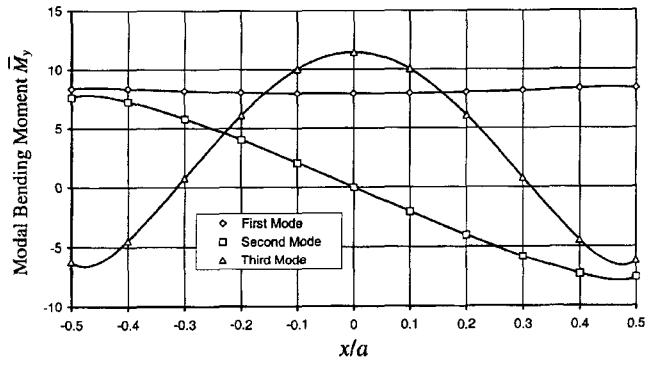

Fig. 12. Closed-form solution of modal bending moment $\bar{M}_y$ versus the coordinate x/a for thick *FSFS* square plate ($h/b = 0.1$) vibrating in the first three modes. The bending moment $\bar{M}_y$ is taken at $y/b = 0.5$.

the plate is thin ($h/b = 0.01$).

All stress-resultants for thin plates are slightly greater than the corresponding stress-resultants for thick plates.

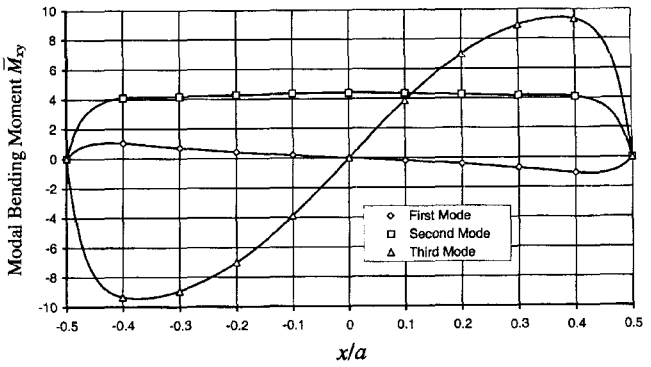

Fig. 13. Closed-form solution of modal twisting moment $\bar{M}_{xy}$ versus the coordinate x/a for thick *FSFS* square plate ($h/b = 0.1$) vibrating in the first three modes. The twisting moment $\bar{M}_{xy}$ is taken at $y/b = 0$.

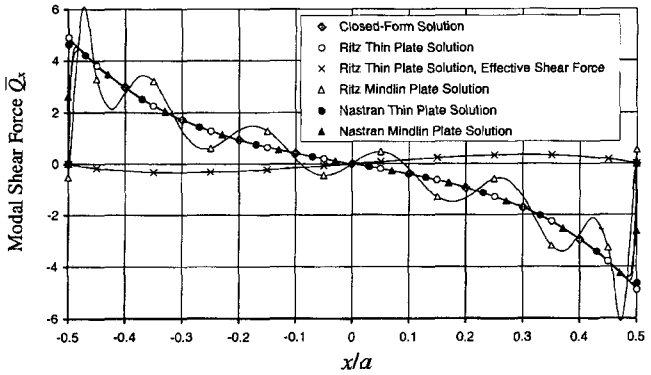

Fig. 14. Closed-form, Ritz and FEM (Nastran) solutions of modal shear force $\bar{Q}_x$ versus the coordinate x/a for thin *FSFS* square plate ($h/b = 0.01$) vibrating in the first mode. The shear force $\bar{Q}_x$ is taken at $y/b = 0.5$.

3.4 Modal Stress-Resultants Prediction by Ritz and FEM Methods

One of the aims of this study is to check the validity and accuracy of the Ritz method and FEM in predicting the modal stress-resultants of plates in the vicinity of free edges. This motivation is prompted by the fact that both the Ritz method and FEM do not impose the natural boundary conditions, namely $Q_x = 0$, $M_x = 0$ and $M_{xy} = 0$, along the free edges. This may cause erroneous predictions for the stress-resultants in the plate.

The stress-resultants $\bar{M}_x$ and $\bar{M}_y$ generated by the Ritz and the FEM methods are in close agreement with the closed-form solutions and are therefore not presented herein. The stress-resultants $\bar{Q}_x$, $\bar{Q}_y$, and $\bar{M}_{xy}$ from the Ritz and FEM methods do not agree well with the closed-form solutions near the free edges of the plates due to the sharp variations of these stress-resultants at the vicinity of the free edges.

Fig. 14 presents the shear force $\bar{Q}_x$, obtained from the

closed-form analytical expression and also from the Ritz method and FEM, for a thin (h/b = 0.01) FSFS square plate. It can be seen that all numerical solutions, except for the ones from the Ritz method using the Mindlin plate theory, are in close agreement with the closed-form solutions for $x/a = -0.45$ to 0.45. The results from the Ritz method show oscillations about the closed-form solutions with varying x/a values. In the vicinity of the free edges ($x = -a/2$ and $x = a/2$), the two Mindlin plate solutions give better prediction than the ones from the two thin plate solutions. The thin plate solutions do not show any trend to approach a zero value at the free edges. The effective shear forces, obtained from the Ritz method using the thin plate theory, however do vanish at the two free edges as shown in Fig. 14.

The relationship of the shear force $\bar{Q}_x$ versus the coordinate x/a for a thick (h/b = 0.1) FSFS square plate is depicted in Fig. 15. The results from the two Mindlin plate solutions are in very close agreement with the ones from the closed-form solution. The two solution methods for the Mindlin plates can be used to predict accurately the transverse shear forces in thick plates. The two solution methods for the Kirchhoff plates are, however, not suitable in analysing thick plates as shown in Fig. 15.

Fig. 16 shows the variations of the twisting moment $\bar{M}_{xy}$ versus the coordinate x/a for a thin (h/b = 0.01) FSFS square plate. All results from the Ritz and FEM solutions are in good agreement with the closed-form solution except near the free edges. In this case, the Mindlin plate solution obtained using NASTRAN gives the best results near the free edges.

The variations of the twisting moment $\bar{M}_{xy}$ versus the coordinate x/a for a thick (h/b = 0.1) FSFS square plate are presented in Fig. 17. The results from the Ritz method and FEM, based on the Mindlin plate theory, are in excellent agreement with the ones from the closed-

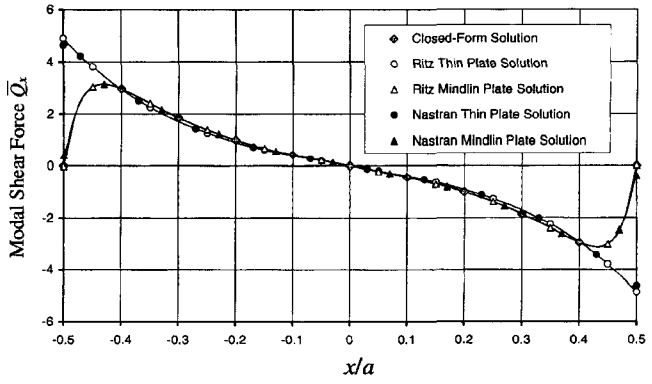

Fig. 15. Closed-form, Ritz and FEM (Nastran) solutions of modal shear force $\bar{Q}_x$ versus the coordinate x/a for thick *FSFS* square plate (h/b = 0.1) vibrating in the first mode. The shear force $\bar{Q}_x$ is taken at y/b = 0.5.

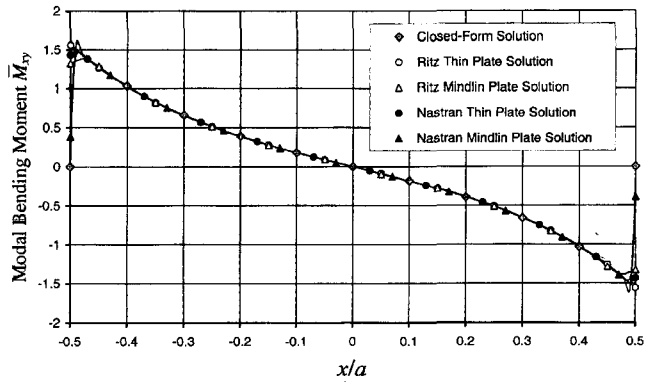

Fig. 16. Closed-form, Ritz and FEM (Nastran) solutions of modal twisting moment $\bar{M}_{xy}$ versus the coordinate x/a for thin *FSFS* square plate (h/b = 0.01) vibrating in the first mode. The twisting moment $\bar{M}_{xy}$ is taken at y/b = 0

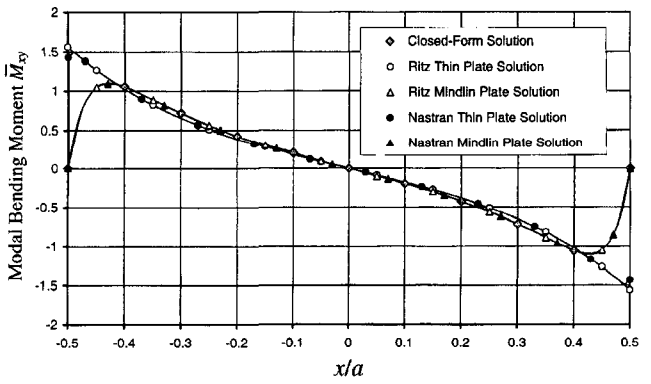

Fig. 17. Closed-form, Ritz and FEM (Nastran) solutions of modal twisting moment M_{xy} versus the coordinate x/a for thick *FSFS* square plate (h/b = 0.1) vibrating in the first mode. The twisting moment M_{xy} is taken at y/b = 0.

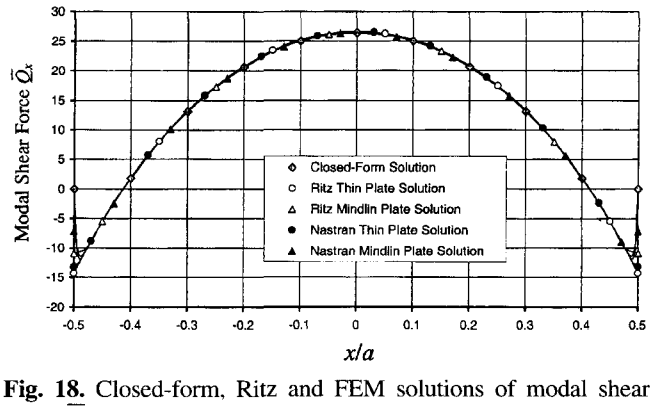

Fig. 18. Closed-form, Ritz and FEM solutions of modal shear force $\bar{Q}_x$ versus the coordinate x/a for thin *FSFS* square plate (h/b = 0.01) vibrating in the second mode. The shear force $\bar{Q}_x$ is taken at y/b = 0.5.

form solutions.

Figs. 18 to 24 present the stress-resultants $\bar{Q}_x$ and $\bar{M}_{xy}$ for the thin (h/b = 0.01) and thick (h/b = 0.1) FSFS square plates vibrating in the second and third modes. It is observed that the Ritz and FEM thin plate solutions fail to predict $\bar{Q}_x$ and $\bar{M}_{xy}$ for thin plates near the free edges (see Figs. 18, 20, 22 and 24) and for thick plates in the entire range of $x/a = -0.5$ to 0.5 (see Figs. 19, 21, 23 and 25). The Ritz method and FEM, based on the Mindlin plate theory, also have problems in furnishing accurate results for thin plates near the free edges. However, these two methods give excellent predictions for $\bar{Q}_x$ and $\bar{M}_{xy}$ in thick plates.

Note: In Figs. 2 to 25, the curves were plotted using 201 equi-spaced sampling points along the horizontal axis for all closed-form solutions, 101 sampling points for the FEM solutions and 41 points for the Ritz solutions. The symbols, on the curves, do not indicate the data points for plotting the curves but they are simply used in identifying the curves.

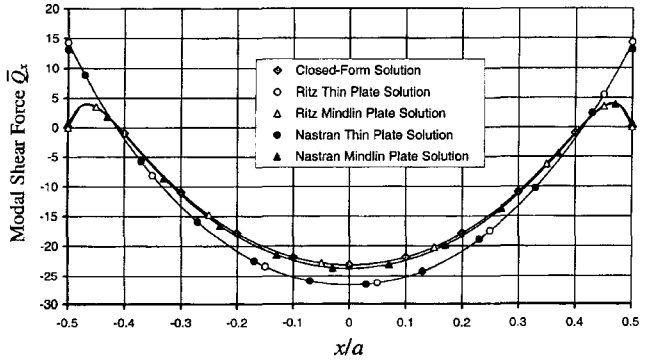

Fig. 19. Closed-form, Ritz and FEM solutions of modal shear force $\bar{Q}_x$ versus the coordinate x/a for thick *FSFS* square plate (h/b = 0.1) vibrating in the second mode. The shear force $\bar{Q}_x$ is taken at y/b = 0.5.

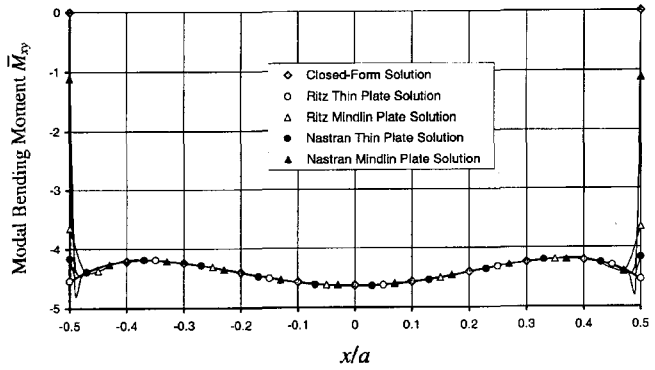

Fig. 20. Closed-form, Ritz and FEM solutions of modal twisting moment $\bar{M}_{xy}$ versus the coordinate x/a for thin *FSFS* square plate (h/b = 0.01) vibrating in the second mode. The twisting moment $\bar{M}_{xy}$ is taken at y/b = 0.

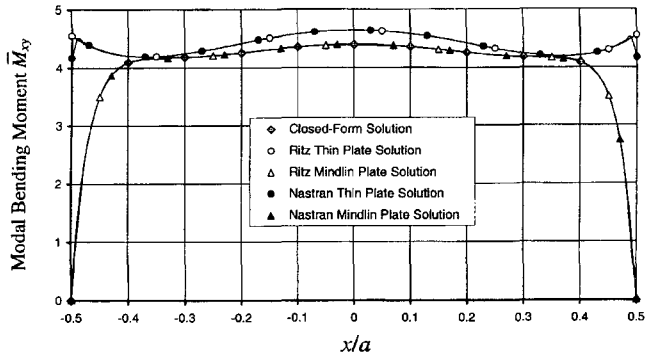

Fig. 21. Closed-form, Ritz and FEM solutions of modal twisting moment $\bar{M}_{xy}$ versus the coordinate x/a for thick *FSFS* square plate (h/b = 0.1) vibrating in the second mode. The twisting moment $\bar{M}_{xy}$ is taken at y/b = 0.

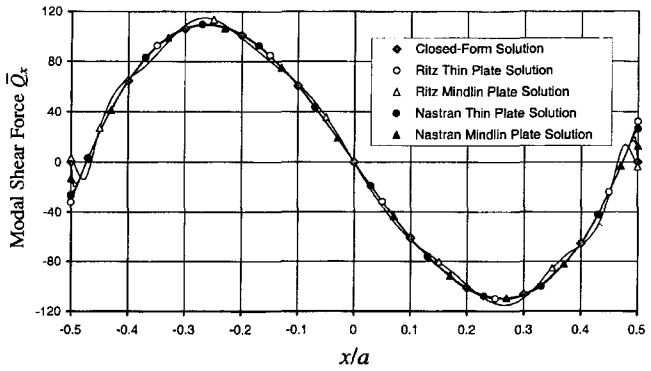

Fig. 22. Closed-form, Ritz and FEM solutions of modal shear force $\bar{Q}_x$ versus the coordinate x/a for thin *FSFS* square plate (h/b = 0.01) vibrating in the third mode. The shear force $\bar{Q}_x$ is taken at y/b = 0.5.

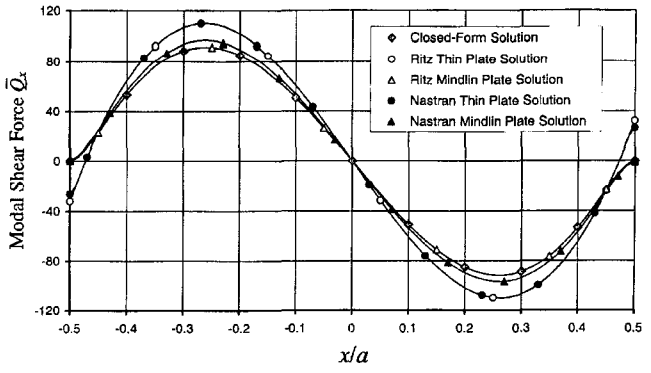

Fig. 23. Closed-form, Ritz and FEM solutions of modal shear force $\bar{Q}_x$ versus the coordinate x/a for thick *FSFS* square plate (h/b = 0.1) vibrating in the third mode. The shear force $\bar{Q}_x$ is taken at y/b = 0.5.

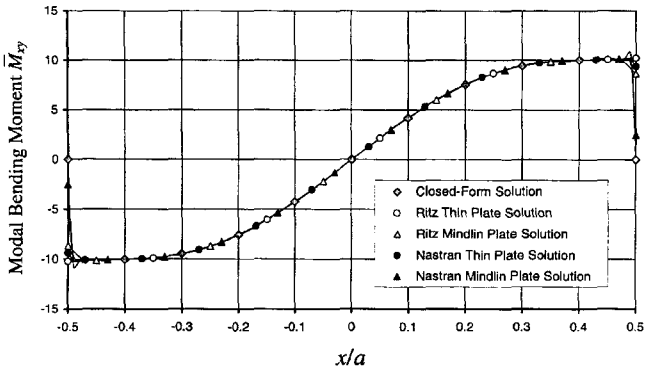

Fig. 24. Closed-form, Ritz and FEM solutions of modal twisting moment $\overline{M}_{xy}$ versus the coordinate x/a for thin *FSFS* square plate ($h/b = 0.01$) vibrating in the third mode. The twisting moment $\overline{M}_{xy}$ is taken at $y/b = 0$.

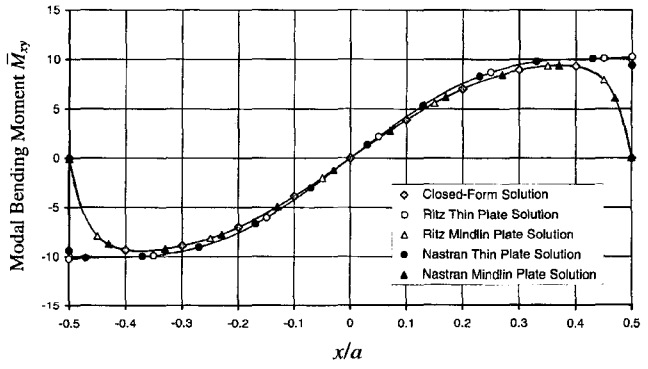

Fig. 25. Closed-form, Ritz and FEM solutions of modal twisting moment $\overline{M}_{xy}$ versus the coordinate x/a for thick *FSFS* square plate ($h/b = 0.1$) vibrating in the third mode. The twisting moment $\overline{M}_{xy}$ is taken at $y/b = 0$.

4. Concluding Remarks

This paper presents exact vibration solutions for rectangular Mindlin plates with two opposite edges simply supported and the other two edges free. The exact modal stress-resultants, hitherto unavailable, provide important benchmark solutions to test the validity, convergence and accuracy of numerical methods in yielding accurate stress-resultants in vibrating plates with free edges.

This paper has also shown that a problem exists in the widely-used Ritz method and finite element method in predicting accurate values of stress-resultants for plates with free edges, especially the transverse shear forces and twisting moments when the plate is thin. Comparing with the closed-form solutions, the shear stress and twisting moment obtained by the Ritz and finite element methods based on the Mindlin plate theory give reasonably accurate results of these stress resultants when the plates are thick. For thin plates, however, both the Ritz method and the finite element method based on the Kirchhoff (thin) and Mindlin (thick) plate theories fail to provide accurate results near the free edges of the plates. Moreover, the stress-resultants such as the shear forces and twisting moments do not satisfy the natural boundary conditions. It is hoped that the findings in this paper will spur researchers to refine both the Ritz method and the finite element method for determining very accurate stress resultant distributions in vibrating plates having free edges. Such a development will be extremely useful to engineers who have to perform hydrodynamic analysis of very large floating structures that may be modeled as plates with all edges free.

References

Chen CC, Kitipornchai S, Lim CW, Liew KM (1999) Free vibration of cantilevered symmetrically laminated thick trapezoidal plates, International Journal of Mechanical Sciences, 41(6): 685-702.

Chen WC, Liu WH (1990) Deflections and free vibrations of laminated plates-Levy-type solutions, International Journal of Mechanical Sciences, 32: 779-793.

Gorman DJ (1982) Free Vibration Analysis of Rectangular Plates, Elsevier North Holland Co.

Gorman DJ, Ding W (1996) Accurate free vibration analysis of the completely free rectangular Mindlin plates, Journal of Sound and Vibration, 189(3): 341-353.

Khdeir AA (1988) Free vibration and buckling of symmetric cross-ply laminated plates by an exact method, Journal of Sound and Vibration, 126: 447-461.

Liew KM, Wang CM, Xiang Y, Kitipornchai S (1998) Vibration of Mindlin Plates: Programming the p-Version Ritz Method, Elsevier Science, Oxford.

Mindlin RD (1951) Influence of rotatory inertia and shear on flexural motion of isotropic elastic plates, ASME, Journal of Applied Mechanics, 13: 31-38.

Utsunomiya T, Watanabe E, Eatock TR (1998) Wave response analysis of a box-like VLFS close to a breakwater, 17th International Conference on Offshore Mechanics and Artic Engineering, ASME, OMAE-98-4331; 1-8.

Xiang Y, Liew KM, Kitipornchai S (1996) Exact buckling solutions for composite laminates: Proper free edge conditions under in-plane loadings, Acta Mechanica, 117: 115-128.